THE JOURNAL OF PHYSICAL CHEMISTRY B
A JOURNAL OF THE AMERICAN CHEMICAL SOCIETY

pubs.acs.org/JPCB

Article

Molecular Dynamics Investigation into pH Dependent Metal Binding of the Intrinsically Disordered Worm Jaw Protein, Nvjp-1

Published as part of The Journal of Physical Chemistry virtual special issue "Honoring Michael R. Berman".

Selemon Bekele,* Kristi Singh, Evan Helton, Sanaz Farajollahi, Rajesh R. Naik, Patrick Dennis, Nancy Kelley-Loughnane, and Rajiv Berry*

Cite This: *J. Phys. Chem. B* 2022, 126, 6614–6623

Read Online

ACCESS | Metrics & More | Article Recommendations | Supporting Information

ABSTRACT: Sclerotization of the *Nereis virens* jaw is mediated by metal binding to the histidine-rich jaw protein, Nvjp-1. Previous studies showed that the mechanical properties of Nvjp-1 hydrogels could be modulated with zinc binding as well as the associated anion. Here, we show that the mechanical properties of Nvjp-1 hydrogels can be modulated by pH and that zinc binding to Nvjp-1 is stable at both acidic and alkaline pH conditions. To probe the mechanism of Zn^{2+} binding to Nvjp-1 at different pH conditions, we utilized all atom molecular dynamics simulations employing a polarizable force field. At low pH conditions, polar residues predominantly interacted with Zn^{2+}, with at most two residues interacting with a given zinc ion. Surprisingly, little to no Zn^{2+} binding was observed with the abundant Nvjp-1 acidic residues, which form salt-bridges with the protonated histidines to effectively block their binding to Zn^{2+} ions. As the pH was shifted to alkaline conditions, Zn^{2+} binding residues reconfigured to form additional coordination bonds with histidine, resulting in a reduction in the radius of gyration that correlated with hydrogel sclerotization. Furthermore, acetate ions were shown to facilitate the capture of zinc ions through association with protonated histidines at low pH, freeing acidic residues to interact with Zn^{2+} ions and increasing the number of Zn^{2+} ions that diffuse into the Nvjp-1 interior. Thus, these studies provide valuable molecular insights into how amino acid residues in Nvjp-1 manage metal salt binding and coordination in hydrogels as a function of the pH and ionic environments.

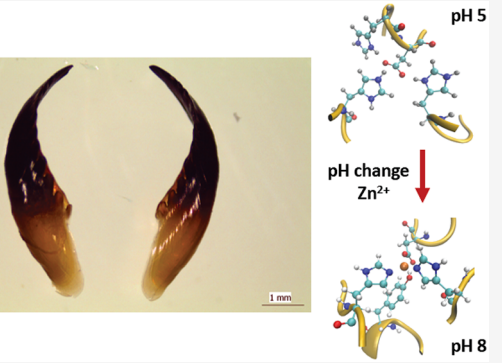

I. INTRODUCTION

There is a growing interest in biomaterials with spatially graded chemical compositions and mechanical properties. Improving the stress distribution at interfaces and minimizing contact deformation are highly desirable in man-made materials and may be achieved by mimicking the structural and chemical properties of biological systems which often prevent damage by employing a smooth transition from hard to soft through mechanical gradients that dissipate large forces.[1] Insights into the relationships between structure and mechanical properties such as hardness, fracture toughness, and wear resistance may be garnered by exploring the properties of hard tissues found in biological organisms to inform design paradigms. This calls for an understanding of the structural and biochemical principles that govern functionality in biological systems through interactions with biotic/abiotic materials to help in the design of synthetic materials with desired properties.

Many of the functional properties of biological materials have been attributed to the presence of metal centers. While calcium based biominerals are responsible for the hardening of teeth and bones in vertebrates, marine invertebrates have also been shown to contain metallized, hard tissues.[2] Invertebrate jaws are different from the more familiar calcified bones and teeth of vertebrates in that they contain high levels of transition metals such as zinc and copper.[2] For instance, the jaws of the marine polychaete *Glycera dibranchiata* contain copper which is present in a crystalline form as the mineral atacamite that is organized into fibers that reinforce the material by enhancing the hardness of the jaw tip.[3] Another example is the *Nereis virens* marine worm jaw which is used for grasping, piercing, and tearing. The jaw was found to exhibit high levels of Zn that correlated with the presence of a highly proteinaceous material enriched in glycine (Gly) and histidine (His).[4,5] Despite the lack of mineralization, the *N. virens* jaw possesses hardness and stiffness properties comparable to human dentin and mechanical properties superior to synthetically engineered polymers.[2] Extensive coordination of Zn^{2+} by a histidine-rich

Received: April 26, 2022
Revised: August 8, 2022
Published: August 25, 2022

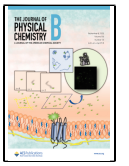

https://doi.org/10.1021/acs.jpcb.2c02807
J. Phys. Chem. B 2022, 126, 6614–6623

protein framework has been shown to be responsible for the remarkable mechanical properties of the *N. virens* jaw, where the nonuniform distribution of the glycine and histidine rich proteinaceous material, in coordination with a 3 wt % zinc content, was shown to be highest at the jaw tip and serrated cutting edge while decreasing gradually to the base.[4,6] This imparts the jaw with mechanical and chemical gradients that greatly enhance functionality.

Proteomic analysis of the *N. virens* jaw material revealed dominant polypeptides at 38 kDa named Nvjp-1, consisting of more than 25 mol % histidine and 35 mol % glycine residues and correlating well with earlier amino acid analyses of the crude jaw material.[5,6] Tyrosine and glutamate/aspartate are also highly represented amino acids present in the Nvjp-1 polypeptide, and it was demonstrated that Nvjp-1 could be recombinantly expressed and purified from *E. coli*.[6] Subsequent studies showed that recombinant preparations of Nvjp-1 could be processed into hydrogels by photochemical and enzymatic cross-linking techniques through the abundant tyrosine residues.[7−9] Placing the Nvjp-1 hydrogels in salt solutions led to condensation and reduced water content, but only treatment with Zn salts resulted in a 2 order-of-magnitude increase in the hydrogel's compressive modulus.[8] As was shown in the natural worm jaw, the metal-mediated increase in mechanical properties was reversible with Zn^{2+} chelation.[10] Furthermore, the choice of anion in the Zn salt had profound effects on the viscoelastic properties of the Nvjp-1 hydrogels. Zinc paired with an acetate ion demonstrated more uniform metallization of the hydrogel but higher levels of stress relaxation and viscous behavior at high strain rates. In the presence of chloride ions, reduced stress relaxation and increased elastic behavior at high strain rates were observed, indicating the stabilization of Zn^{2+} coordination bonding with chloride. This is consistent with earlier observations that zinc levels in the worm jaw closely correlate with that of Cl^-, and the presence of His approximately follows Zn^{2+} and Cl^- concentrations.[10,11] Combining this information with extended X-ray absorption fine structure (EXAFS) and X-ray absorption near edge structure (XANES) data, it has been suggested that zinc acts as a cross-linker of the proteinaceous matrix by forming $Zn(His)_3Cl$-like units.[4] Together these observations indicated coordination of Zn^{2+} by His residues and chloride and showed that the presence of Nvjp-1 is sufficient to explain the effects of metal binding on worm jaw mechanical properties.

It is difficult to experimentally determine which residues in Nvjp-1 are interacting with Zn^{2+} under different environmental conditions. As an initial approach to this problem, Chou et al.[7] carried out a multiscale computational study of the Nvjp-1 protein where they employed density functional theory (DFT) calculations, replica exchange molecular dynamics (REMD) simulations, and a coarse-grained elastic network model to elucidate the role played by metal coordination in Nvjp-1 cross-linking mechanisms. The results from DFT analysis, which involved different complexes of histidine with Zn^{2+}, indicated that the highest occupied molecular orbital (HOMO) and the lowest unoccupied molecular orbital (LUMO) are mostly localized in the histidine side chains rather than in the Zn^{2+} ions. This suggests a mostly electrostatic interaction between the positively charged ions and the lone pairs of electrons of either oxygen or nitrogen atoms.

While the DFT study implied interactions between Zn^{2+} and lone pairs on atoms of the protein, the REMD simulations involved the nonpolarizable CHARMM force field for protein atoms and the TIP3 water model where polarization effects are accounted for in a mean-field manner by fixing partial atomic charges of the system to effective values which remain fixed throughout a simulation. The REMD simulations predicted different mechanical responses as a function of changing ion concentrations. However, it is well-known that the charge distribution of a molecule can change in response to its environment; i.e., molecules are polarizable.[12] For example, the conformation of a peptide affects its electronic distribution,[13] and the electronic distribution of a ligand changes upon binding to a protein.[14] Neither of these effects would be captured by a nonpolarizable force field. For *ex vivo* processing of Nvjp-1 into reconfigurable materials, we were interested in determining how metal binding of the protein could be modulated by changing the pH environment and the presence of the metal salt counteranion. Here we show that stable binding of Zn^{2+} metal ions in Nvjp-1 hydrogels allows the mechanical properties of the hydrogels to be modulated by shifting the pH conditions of the environment without additional exposure to the metal. To probe how the Nvjp-1 protein manages Zn^{2+} ion binding through varying pH conditions, as well as the effect of the anion partner of Zn^{2+}, all atom molecular dynamics (MD) simulations were employed using a polarizable force field where each of the Nvjp-1 structures was solvated in zinc chloride and zinc acetate solutions for a total of 10 simulations. The results of these studies suggest a system where polar residues mediate metal binding at low pH conditions and pass them to a carboxylate/imidazole coordination pocket as the pH approaches neutrality in $ZnCl_2$. To the best of our knowledge this work is the first computational study of the Nvjp-1 protein in microscopic detail where polarization effects are taken into account explicitly.

II. MATERIALS AND METHODS

Expression and purification of Nvjp-1 were performed according to a previously published method.[8] The enzymatic cross-linking of Nvjp1 hydrogels was carried out as described earlier.[8,9]

Nvjp-1 Mechanical Testing. The mechanical testing of Nvjp-1 hydrogels was performed using a CellScale MicroTester G2 using parallel plate compression. Hydrogels were kept within a bath of the respective buffer at room temperature throughout testing. The instrument was operated using the displacement control in ramp mode, which applies the displacement at a constant nominal rate. The cycle test parameters were set to ramp to a 5% strain over 30 s, followed by a 1 s hold time and a 30 s unload. The data and images were both captured at a frequency of 5 Hz. Young's modulus was calculated using E = stress/strain = $(F/A)/(\Delta L/L_0)$ where E is the Young's modulus; F is the force applied; A is the area through which the force is applied; ΔL is the displacement and L_0 is the initial position of the compression plate. The slope of the stress−strain curve is calculated using the least-squares method for determining the best fit for the data. Experiments were performed on at least three different hydrogels, and the standard error was calculated.

Metal Analysis of Hydrogels. Energy dispersive spectroscopy (EDS) was used to estimate the zinc content of the hydrogels. EDS analysis was performed using a Zeiss Gemini

https://doi.org/10.1021/acs.jpcb.2c02807
J. Phys. Chem. B 2022, 126, 6614−6623

500 SEM equipped with an Xmax 80 detector by Oxford Instruments operated at an acceleration voltage of 15 kV for the measurements. The raw data were analyzed using Aztec software to determine the elemental composition and atomic percentages of each element. Data were accumulated from three areas on each hydrogel and the results averaged.

Structure Modeling. The Rosetta[15] macromolecular modeling program was used to generate the initial structure of the Nvjp-1 protein. The methods employed in the program optimized the value of an energy or scoring function to generate an ensemble of structures with conformations corresponding to energies close to the global energy minimum. Conformational variation in the target protein structure was achieved by inserting fragments of nine or three residues taken from a preselected fragment library starting from a linear conformation of the target sequence. Different clustering algorithms were used to obtain five model structures. An example of the three-dimensional Nvjp-1 structure is shown in Figure S1 of the Supporting Information.

Force Field. The CHARMM force field modified to include polarization effects by incorporating the Drude polarizable force field was used.[16−21] The system prepared according to the specifications outlined was then submitted to the CHARMM-GUI[22,23] web server to generate the necessary input files for simulations. All simulations were carried out using the NAMD (nanoscale molecular dynamics) package.[24] The simulations incorporated polarization effects by adding the so-called Drude particles to all the heavy atoms in the system for simulation with the Drude polarizable force field. The system before the addition of the Drude particles, i.e., without polarization, was subjected to a sufficiently long minimization to ensure the system will have no particle overlap when adding Drude particles.

The SWM4-ND polarizable model was used to simulate water.[25] Nonbonded interactions were modeled by means of dispersive and electrostatic forces. The electrostatic interactions were modeled by a Coulombic potential with long-range corrections treated using the particle mesh Ewald (PME) method.[26,27] A 12−6 Lennard-Jones (LJ) potential was used to model dispersive interactions with the LJ parameters for unlike interactions determined by Lorentz−Berthelot mixing rules.[28] The cutoff distance for all interactions was 12 Å.

The dimensions of the simulation box were chosen so that periodic images of the Nvjp-1 protein did not interact with each other, and periodic boundary conditions were applied in three dimensions. The simulations were performed in the canonical *NPT* ensemble at a pH of 5 and 8 and a temperature of 500 K. The higher temperature was chosen to enhance the mobility of the ionic species in the system and hence obtain data in a reasonable amount of time instead of running at room temperature which would entail prohibitively long simulation times. The temperature is well below the degradation temperature of Nvjp-1, and its disordered nature is also not affected. The Langevin thermostat[29,30] with a relaxation time of 100 fs was used to keep the system temperature fixed at 500 K. The equations of motion were solved using the velocity-Verlet algorithm with a time step of 0.5 fs. Trajectory data were saved every 25 ps.

Nvjp-1 Simulation Setup. To mimic the pH environment of Nvjp-1, PROPKA[31,32] was first used to create models of Nvjp-1 with protonation states corresponding to different pH values. Supporting Information Figure S2 shows the protonated fraction as a function of pH as calculated by PROPKA for histidine and acidic residues. At physiological pH, about 50% of the histidines are protonated and almost all the acidic residues (aspartates and glutamates) are deprotonated (Supporting Information Figure S2a,c). As expected, the histidines become progressively deprotonated at pH values greater than 6, existing predominantly in the δ form. When the Nvjp-1 protein is introduced into a solution containing zinc ions, initially no ions would be present in the interior of the protein. To replicate this condition in the simulation, the volume occupied by the protein was determined in order to keep ions outside the protein at the beginning of a simulation. For this purpose, distributions of distances for histidine imidazole nitrogen and acidic residue carboxylic oxygen, with respect to the center of mass of the protein, were built as these would potentially be on the surface of the protein because of their hydrophilic character (Supporting Information Figure S3). The distributions for nitrogen and oxygen have very similar peak positions and widths, so there was likely no bias by randomly placing the ionic species outside the protein in terms of which residues may capture zinc ions first. Based on the plots in Supporting Information Figure S3, ions within a 50 Å radius from the center of mass of the protein were excluded. The rest of the simulation volume needs to have a sufficient number of zinc cations and anions to make sure the whole system remained neutral. We started with a sufficiently large number of ions in the simulation box, removing all the ions within a specified radius from the protein center of mass, and then randomly removed ions from the rest of the system volume until the concentration reached a value of 200 mM. At pH 5, acetate has a larger pK_a value than ASP and GLU. At this pH, the ratio of the ionic form to the acidic one is approximately 1.76:1 which implies there would be excess acetate ions over the acidics. To make matters simple, we have not modified the protonation state of the acetate ions dissociating from $Zn(OAc)_2$. See section 1 of the Supporting Information for more details.

III. RESULTS AND DISCUSSION

Mechanical Testing of Nvjp-1 Hydrogels. In studying the conditions necessary for the metal loading of Nvjp-1 cross-linked hydrogels, we tested whether the hydrogels could bind zinc under low pH conditions in sufficient amounts to support hydrogel sclerotization when the pH was raised. Nvjp-1 solutions (3 wt % Nvjp-1, 5% glycerol) were enzymatically cross-linked with horseradish peroxidase as described previously and air-dried (Figure 1a), followed by rehydration in 200 mM NaOAc or 300 mM $Zn(OAc)_2$ solutions at pH 5 (Figure 1b).[8,9] The metallized hydrogels were then soaked in NaOAc buffer at pH 5 to remove any unbound zinc (Figure 1b). Mechanical testing of the resulting hydrogels demonstrated little to no increase in the compressive modulus with the Zn^{2+} treated hydrogels when compared to the Na^+ control, consistent with the idea that the histidines are largely protonated at this pH. As the hydrogels were moved to NaOAc, pH 7, the Zn^{2+} treated hydrogels demonstrated a significant increase in compressive modulus, where only a minor increase in mechanical properties was observed with the Na^+ control (Figure 1b).

Shifting the pH to 8 resulted in a further increase in compressive modulus with the zinc treated hydrogel. When the pH was adjusted back to 5, the compressive moduli of both Na^+ and Zn^{2+} treated hydrogels reverted to the initial pH 5 values. EDS analysis was used to determine how the zinc levels

https://doi.org/10.1021/acs.jpcb.2c02807
J. Phys. Chem. B 2022, 126, 6614−6623

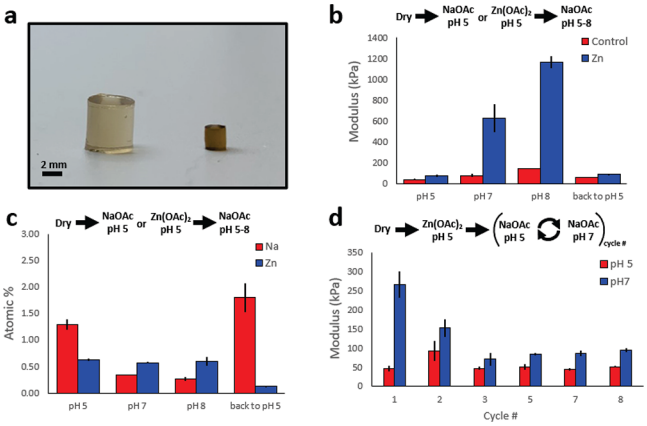

Figure 1. (a) Enzymatically cross-linked Nvjp-1 protein hydrogels after demolding (left) and drying (right). The dried hydrogels are processed according to the scheme shown in (b). Results from the mechanical testing of the hydrogels incubated in Zn^{2+} and the controls are shown in (c) where error bars represent the standard error. The numbers displayed above the modulus values for the Zn^{2+} samples represent the atomic % of Zn^{2+} as determined by EDS analysis. (d) Hydrogels were metallized with zinc at pH 5 followed by multiple rounds of cycling in sodium acetate buffer from pH 5 to 7. Mechanical properties of the hydrogels were measured after each pH change.

changed as the hydrogels were moved through the different pH conditions. After soaking in NaOAc at pH 5, the zinc bound hydrogels were found to contain a 0.64 atomic % of Zn^{2+} (Figure 1c). This level did not change significantly as the hydrogels were placed at a neutral (pH 7) or alkaline (pH 8) conditions. However, Zn^{2+} levels dropped significantly when the pH was adjusted from 8 back to 5, corresponding to the decrease in compressive modulus observed in Figure 1b. This was confirmed when Zn^{2+} treated hydrogels were cycled numerous times between pH 5 and pH 7. In this experiment, Zn^{2+} mediated effects on compressive modulus dissipated quickly after the first cycle, reaching a stable baseline by cycle 3 (Figure 1d). Together the data indicate that Nvjp-1 hydrogels can be metallized at a low pH to effectively enhance their mechanical properties with increasing pH. This trend does not work in reverse, suggesting the mechanisms of metal binding and metal transfer by Nvjp-1 at the different pHs are asymmetrical.

Nvjp-1 Zinc Binding at pH 5. Molecular dynamics simulations were performed at a pH of 5 in order to understand how Nvjp-1 might be metallized under low pH conditions. Nvjp-1 is rich in glycine, histidine, tyrosine, and acidic amino acids (aspartate and glutamate). The pK_a of histidine is about 6.0 which corresponds to the pH where the number of protonated histidines are equal to the neutral side chain. At a pH of 5, 80% of the Nvjp-1 histidines are protonated making them positively charged (Supporting Information Figure S2a). At this pH, the zinc ions cannot interact with the positively charged histidine residues for coordination due to electrostatic repulsion. On the other hand, almost 90% of the acidic residues are negatively charged at a pH of 5. All results presented in this work are from simulations run for over 300 ns. The equilibration of the Nvjp-1 protein is illustrated in the plot of the root-mean-square deviation (RMSD) as a function of time (see Supporting Information Figure S4). Coordination between the carboxylic oxygens and the positively charged zinc ions was anticipated purely on the basis of attractive electrostatic interaction between positive and negative charges. Contrary to expectation, the simulation results indicated the majority of the aspartate and glutamate residues did not make coordination bonds with zinc ions. In contrast, polar residues were consistently observed to capture zinc ions from the solution and remain coordinated with them throughout the length of the 300 ns simulation time. This is readily explained if the hydration of ions by water is considered. Water molecules are naturally polar and can interact with ions as a result of charge redistribution in response to the electric field produced by the ions. Similarly, hydroxyl and amine groups on polar but neutral residues can interact with ions as a result of polarization even though they do not have overall explicit charge.

Figure 2 shows example snapshots of polar and protonated acidic residues coordinating with the positively charged zinc

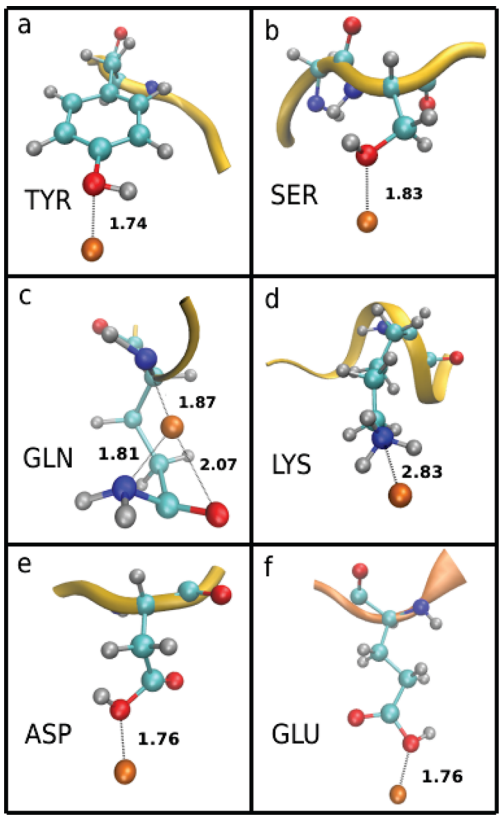

Figure 2. Shown are examples of Zn^{2+} coordination with the hydroxyl containing TYR and SER (a, b), the amine nitrogens on GLN and LYS (c, d), and the protonated acidic residues ASP and GLU (e, f). The distances shown are in angstroms. Unless specified otherwise, the colors of atoms in the snapshots are such that oxygens are red, hydrogens are white, nitrogens are blue, carbons are cyan, and zinc ions are orange. The water molecules, counterions, Drude particles, and lone pairs in the system are not shown for clarity.

ions. The distances shown are in angstroms and correspond to peak positions obtained by fitting distance distributions to Gaussian functions (see Figure S5). The heavy atoms have Drude particles attached to them whose motions, as the result of their response to imposed electric fields, mimic charge redistribution in real systems. At pH of 5, 10% of the acidic residues are protonated which would be expected to preclude any coordination with the positively charged zinc ions. However, in addition to the polar residues(Figure 2a–c), the

https://doi.org/10.1021/acs.jpcb.2c02807
J. Phys. Chem. B 2022, 126, 6614–6623

protonated residues are also observed to coordinate with zinc ions (Figure 2e,f). Closer inspection of these cases revealed that polarization of the hydroxyl oxygens is responsible for the coordination (Supporting Information Figure S6a). Similarly, the positively charged zinc ion may interact with a positively charged lysine residue as a result of the polarization of the amine nitrogen and the zinc ion (Supporting Information Figure S6b) in addition to the polarization of atoms on side chains of nearby residues. Zn^{2+}−residue coordination occurs in a complex environment which results in a distribution of configurations. Examples are shown for GLU in Figure S7.

Table T1 in the Supporting Information shows a comparison of interaction energies between Zn^{2+} and various residues from the Drude model and DFT. The energies from DFT correspond to the structures optimized in vacuum using Gaussian16[33] and calculated as $E_{int} = E_{complex} - (E_{residue} + E_{zn})$. Optimized structures for some selected residues are shown in Figure S8. The DFT calculations predict binding of Zn^{2+} to the residues shown in Figure 2 except for LYS. The differences between the DFT energies and those from the Drude model are in the range 5−67 kcal/mol. However, an exhaustive combination of levels of theory and basis sets needs to be explored in order to check if better agreement with the Drude model can be obtained. We would like to note that the energies from the Drude model are for Zn^{2+}−residue interactions in an aqueous environment with several residues, water molecules, and anions in the vicinity of Zn^{2+} while those from DFT are gas phase calculations for Zn^{2+} interacting with a single residue. The CHARMM Drude force field uses ion parameters developed with ions solvated in water. As a result, direct comparison may not be warranted. We would like to emphasize at this point that the development of ion parameters for use with protein residues is necessary for realistic simulations where good agreement between DFT and Drude ion−residue interaction energies may be obtained.

Role of Nvjp-1 Acidic Residues at Low pH. At a pH of 5, the acidic residues in Nvjp-1 do not coordinate with zinc ions to a large extent, with the exception of a small number of protonated carboxylic acids. To address this counterintuitive result, we looked into whether the protonated histidines (HSP) are somehow influencing the acidic residues, by preventing them from interacting with the zinc ions. In order to see if there is any association between acidic and protonated histidines, we calculated the radial distribution function between carboxylic oxygen and imidazole nitrogen (Figure 3a,b). It is evident from these plots that acidic residues are indeed interacting with the histidines and the distances between the pair of atoms in the first $g(r)$ peak are suggestive of hydrogen bonding between the acidic oxygens and the δ or ε hydrogens bound to the imidazole nitrogens. The association between acidic side chains and protonated histidine residues is indicated in example snapshots (Figure 3c,d), where the aspartate and glutamate residues are each surrounded by three histidines.

Considering that the histidines have one unit of positive charge and an acidic residue has one unit of negative charge, the overall charge of the assembly is positive and produces a region of high potential from which the positively charged zinc ions would be repelled. To confirm this, we looked into the nonbonded interactions between zinc ions and the associating acidic and histidine residues. The distribution of the nonbonded (van der Waals + Coulomb) interaction energies between zinc ions and several associated acidic and protonated

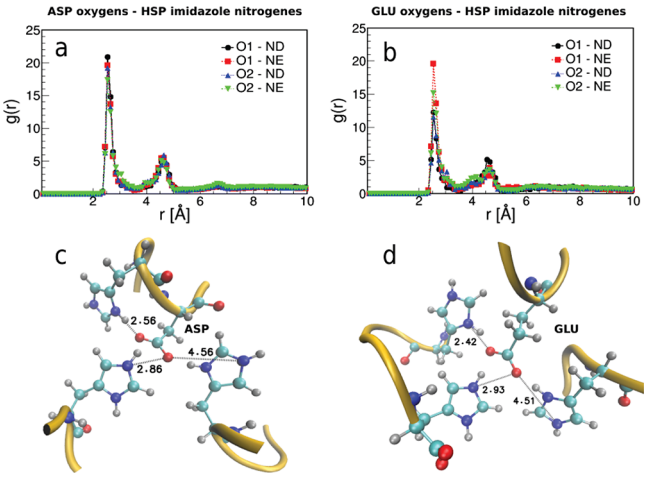

Figure 3. (a, b) Radial distribution functions between carboxylic oxygens and δ or ε nitrogens of the protonated histidines (HSP): ND, δ hydrogen; NE, ε nitrogen. (c, d) Association of acidic residues with protonated histidines: (left) aspartate; (right) glutamate. The distances shown are in angstroms. One of the histidines is a close neighbor.

histidines shows that the energies are mostly positive for the various acidic + histidine combinations, further supporting the idea that the zinc ions experience a positively charged region wherever the acidic residues are located (Figure 4). In the

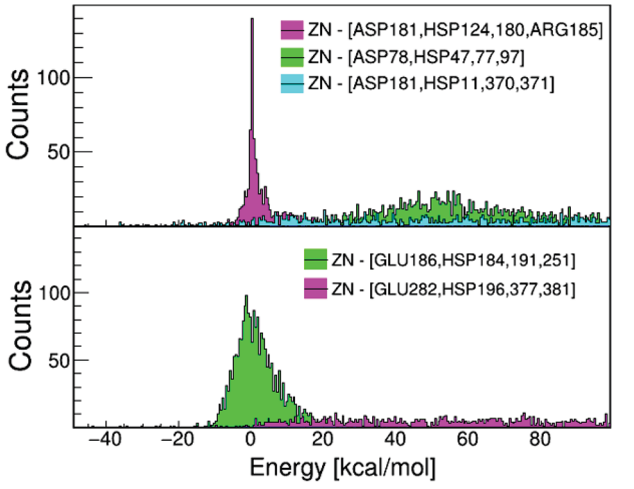

Figure 4. Nonbonded (van der Waals + Coulomb) interaction energies between zinc ions and associating acidic and protonated histidines: (top) Zn with ASP + HSP; (bottom) Zn with GLU + HSP.

cases where the interaction energy is close to zero or slightly negative, there may not be a sufficient driving force that leads to zinc ion coordination with the acidic residues. Taken together, the simulations suggest that at low pH, the protonated histidines preform a metal binding pocket by associating with the acidic side chains, whereas metallization is primarily mediated by the polar amino acids.

Role of Acetate vs Chloride in Zinc Binding at pH 5. Previous studies showed that the anion partner of zinc salts played an important role in the metallization of Nvjp-1 hydrogels.[8] When chloride was used as the initial metallizing counteranion, zinc was found to bind Nvjp-1 hydrogels tightly, creating a hard outer shell that ruptured under strain. However, when acetate was used as a counteranion, the zinc

https://doi.org/10.1021/acs.jpcb.2c02807
J. Phys. Chem. B 2022, 126, 6614−6623

was able to penetrate the hydrogels more readily, leading to even metallization throughout the hydrogel. To determine how the anion partner affects zinc ion coordination, the number of zinc ions inside the Nvjp-1 was calculated as a function of time with either chloride or acetate as a counteranion (Figure 5a).

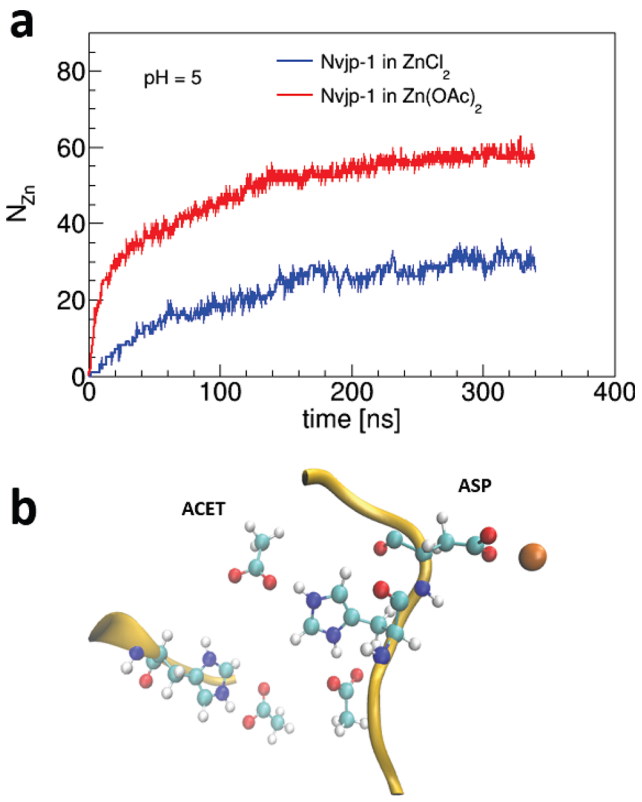

Figure 5. (a) Number of zinc ions as a function of time inside the Nvjp-1 in $ZnCl_2$ and $Zn(OAc)_2$ solutions at pH = 5. A distance cutoff of 3 Å between zinc ions and oxygen or nitrogen atoms of residues is used for the counting. (b) Snapshot of associated acetate ions with protonated histidines in the presence of $Zn(OAc)_2$ allowing the aspartate residue to interact with a zinc ion.

Snapshots of the zinc ion distribution in equlibrated Nvjp-1 structures are shown in Supporting Information Figure S9. A distance cutoff of 3 Å between zinc ions and oxygen or nitrogen atoms of residues is used for the counting. For both solutions, the number of coordinating zinc ions initially increased over the first 150 ns of simulation, before saturating over time. However, the rate was faster in zinc acetate, reaching a value of $N_{Zn} \sim 25$ in the first 20 ns, whereas with zinc chloride it took ~150 ns to attain the same value. Additionally, the average saturated value of zinc ion coordination in the presence of acetate is almost twice that observed in the presence of chloride. The acetate counteranion is chemically similar to aspartate and glutamate side chains that were shown to associate with the protonated histidines at pH 5 (Figure 3a,c). In the simulation, an acetate ion from $Zn(OAc)_2$ substitutes for a histidine-associated aspartate residue, allowing the aspartate residue to interact with a zinc ion (Figures 3c and 5b). Thus, acetate ions indirectly help the transport of zinc ions into the interior of Nvjp-1, as the negatively charged acidic residues are freed from their association with the protonated histidines and help to attract the more positively charged zinc ions.

Zinc, Counterions and Nvjp-1 Radius of Gyration at Varying pH. Chou et al. demonstrated that hydrogel contraction increased with zinc coordination compared to contraction in the presence of sodium, and this was attributed to the larger number of cross-links that occurred in the presence of zinc. Through MD simulations, we looked to see how changing pH and the counteranion species might affect Nvjp-1 contraction in the presence of zinc. The radius of gyration (R_g) provides information on the size and compactness of protein molecules. Here we investigated how the R_g of Nvjp-1 responds to zinc metallization under acidic and alkaline pH conditions as a function of chloride or acetate as the counteranion. When metallization occurs in the presence of $ZnCl_2$ at pH 5, the R_g of Nvjp-1 appears to decrease at early times from its starting value but fluctuates strongly over time (Figure S10a, red). This can be explained by the prior observation that the majority of acidic residues are bound with the protonated histidines and do not make coordination bonds with zinc ions. Rather, polar residues are primarily involved in the capture of zinc ions from the solution, where coordination by polar side chains persists throughout the simulation time. When the pH is shifted to 8, the Nvjp-1 R_g stabilizes (Figure S10a, blue) and the R_g distribution is narrower, indicating a contraction of Nvjp-1 due to an increase in coordination with zinc ions (Figure 6a). It should be noted at this point that no

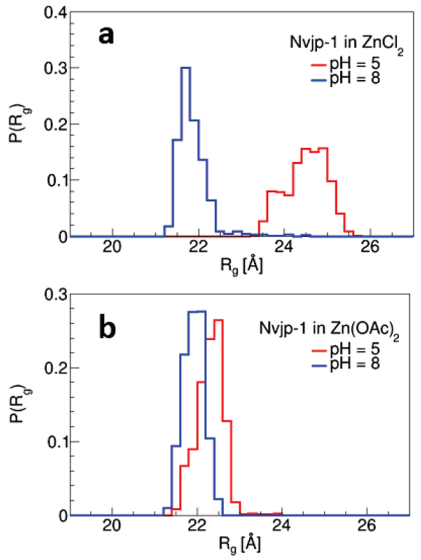

Figure 6. Nvjp-1 radius of gyration distributions at pH 5 (blue) and pH 8 (red): (a) in $ZnCl_2$; (b) in $Zn(OAc)_2$.

additional zinc ions were added to the system when it was shifted from pH 5 to 8. In contrast, the R_g of Nvjp-1 metallized in zinc acetate, at pH 5, shows a decrease at early times but attains an average value with much smaller fluctuations (Figure S10b). However, the R_g distribution is substantially narrower in the presence of acetate than with chloride at pH 5. Nvjp-1 metallized in zinc acetate also shows a narrowing of the R_g distribution when the pH is shifted to 8, but the shift is smaller compared with zinc chloride (Figure 6b). This may be explained by a higher number of acidic and polar residues interacting with zinc at pH 5 in the presence of acetate compared to chloride. The differences in the R_g distributions suggest that the larger equilibrium number of zinc ions coordinating with the Nvjp-1 in the presence of acetate is likely

https://doi.org/10.1021/acs.jpcb.2c02807
J. Phys. Chem. B 2022, 126, 6614−6623

the reason for the smaller fluctuation of R_g (Figure S11). As the pH shifts to more alkaline levels, this results in a greater coordination of zinc ions with histidine and acidic side chains further stabilizing the protein structure.

pH and Counteranion Effects on Zinc Coordination. To gain insights into how pH and counteranions influence the R_g of Nvjp-1 during metal binding, we studied how the coordination state of Nvjp-1 changed with changing conditions. Looking at the time averaged count of residues that coordinate with zinc ions in $ZnCl_2$ and $Zn(OAc)_2$ solutions, it is clear from the raw counts that the residues participating in capturing zinc from solution at pH 5 are different in the presence of acetate or chloride anions (Figure 7a,b). We note at this point that the total numbers of zinc ions

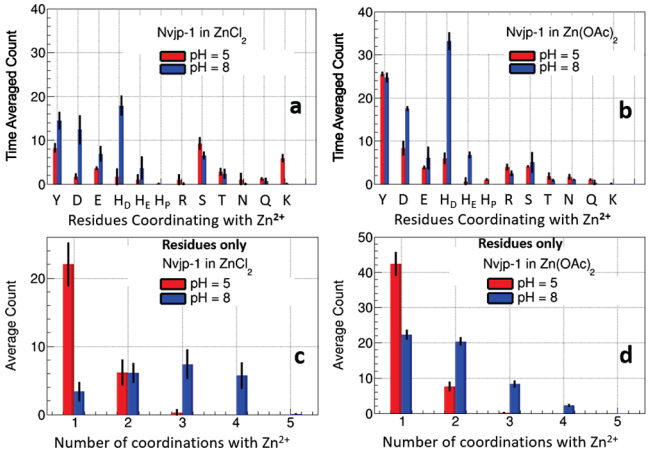

Figure 7. (a, b) Raw count of residues coordinating with Zn^{2+} in $ZnCl_2$ (left column) and $Zn(OAc)_2$ (right column). H_D and H_E represent histidines with hydrogens on the δ and ε nitrogens, respectively. H_P denotes the protonated histidens. (c, d) Number of coordinations with a given Zn^{2+} counting only protein residues.

in the two systems are the same. The only difference is in how many zinc ions were able to make coordinations with the Nvjp-1 protein and which residues are involved. Figure S12 in the Supporting Information shows the normalized fractions of coordinations with a given Zn^{2+}. In the presence of the chloride anion, the top three Zn^{2+} binding residues are TYR, SER, and LYS (Figure 7a). The reduced role for acidic residues in Zn^{2+} binding is expected due to the formation of salt bridges with the 75% protonated histidines at pH 5 as shown previously. As a result, the acidic residues do not coordinate with zinc ions, even though 90% are negatively charged. Alternatively, with acetate as the Zn^{2+} counterion, TYR, ASP, and HIS are the top three Zn^{2+} binding residues (Figure 7b), with the largest increases observed for TYR and ASP binding. About a third of the acidic residues become free to coordinate with zinc ions in zinc acetate at pH 5, stemming from the acetate's faster mobility, chemical similarity of its carboxylic group to the acidic residues, and ability to interact with the protonated histidines.

Zinc ions are mostly coordinated with four ligands at pH 5 in the presence of chloride, looking at the coordination number of Zn^{2+} counting water, counterions, and protein residues (Supporting Information Figure S13a), a number that does not change when the pH is shifted from 5 to 8. In the presence of acetate at pH 5, the coordination number of zinc is largely 3−4 but shifts to slightly higher coordination numbers when the pH changes to 8 (Supporting Information Figure S13b). As the coordination number of Zn^{2+} in a proteinaceous environment is expected to be 4,[4] these results indicate that the counterions and water molecules satisfy the coordination needs of Zn^{2+}.

When the pH is transitioned from 5 to 8, with no additional zinc ions added to the system, the coordination of zinc ions increases from 1−2 residues (Figure 7c,d) to 1−4 in the presence of chloride or acetate after a simulation of over 300 ns. The number of cases with one residue coordination decreased by 70% and those with two residue coordination was reduced by about 15% when switching from pH 5 to pH 8 in the presence of chloride. This increase is likely due to the deprotonation of histidines in Nvjp-1, breaking salt bridges formed with the acidic residues and freeing the acidics and histidines to interact with the zinc ions that were previously bound to polar side chains at pH 5. In contrast to the model $Zn(His)_3Cl$ proposed in the literature for sclerotization of the Nvjp-1,[4,8] the model presented in this work suggests a combination of polar acidic and histidine residues interacting with Zn^{2+} at high pH. Although Nvjp-1 in $Zn(OAc)_2$ at pH 5 (Figure 7b) demonstrates a larger number of residues coordinating with zinc ions and a larger fraction of free acidic residues, the coordination number is limited to at most two residues (Figure 7d), similar to the situation in $ZnCl_2$ at the same pH. When Nvjp-1 in the presence of zinc chloride is shifted to a pH of 8 (Figure 7c), coordination numbers of 3−4 residues per Zn^{2+} increased. In contrast, the number of cases with 3 and 4 coordination per Zn^{2+} did not increase as dramatically when shifting to pH 8 in the presence of acetate (Figure 7d). Inspection of the coordination data indicates that the acetate ions coordinating with a given zinc ion at pH 5 effectively shield it from interaction with the carboxylic and histidine residues at pH 8. The implication of this intriguing result is that sclerotization of the Nvjp-1 in zinc acetate is not as efficient as in zinc chloride. This may be due to the ability of the mobile acetate ions to respond to external stimulus relative to the bulkier and sterically constrained protein side chains and may explain the deformability of the Nvjp-1 hydrogel observed after treatment with zinc acetate.[8]

It has been mentioned earlier that zinc acts as a cross-linker of the proteinaceous matrix by forming $Zn(His)_3Cl$-like units.[4] However, as shown in Figure S8 and Figure 7c,d, counterions and water molecules are needed in addition to protein residues to satisfy the coordination needs of Zn^{2+}. Also, whenever Zn^{2+} is coordinating with protein residues in Nvjp-1, it is not exclusively with histidines. Figure 8 shows various possibilities for interaction with zinc. Panel a displays a zinc ion interacting with HSD, TYR, and two ASP. In panel b, we see that ASP, TYR, and two HSD are coordinating with zinc. Panel c exhibits zinc coordinating with four different residues: ASP, HSE, TYR, GLU. Panel d shows an example of three residues and a chloride ion interacting with Zn^{2+}. Altogether, these results show that residues other than histidines may also play a role in sclerotization of the Nvjp-1 hydrogel.

IV. SUMMARY

In this work, sclerotization of Nvjp-1 in the presence of Zn^{2+} was investigated by all atom molecular dynamics simulations that employed a polarizable force field. The protonation state of the protein determines which types of residues capture zinc ions from solution. At pH 5 in $ZnCl_2$, polar residues are predominantly interacting with Zn^{2+} forming coordination

https://doi.org/10.1021/acs.jpcb.2c02807
J. Phys. Chem. B 2022, 126, 6614−6623

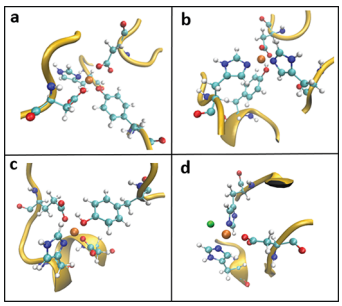

Figure 8. Snapshots of a zinc ion coordinating with four residues: (a) ASP, ASP, HSD, TYR; (b) ASP, HSD, HSD, TYR; (c) ASP, HSE, TYR, GLU. (d) A chloride ion and three residues: ASP, HSD, TYR, Cl^- at pH 8.

bonds and at most two residues are observed to interact with a given zinc ion. At this pH, the negatively charged acidic residues form salt-bridges with protonated histidines and are effectively unavailable for binding with zinc ions. Changing the protonation state of Nvjp-1 to reflect a pH of 8 resulted in a reconfiguration of the coordinate bonds where up to four residues interact with a given zinc ion. This leads to an accompanying reduction in the radius of gyration which may be taken as an indication of sclerotization. Additionally, the effect of the zinc salt anion partner was studied with metallization of Nvjp-1 at pH 5. The acetate ion has been observed to facilitate the capture of more zinc ions by associating with protonated histidines, essentially freeing some acidic residues to interact with zinc ions and increasing the number of zinc ions that diffuse into the Nvjp-1. With more zinc ions interacting with residues, the radius of gyration with $Zn(OAc)_2$ was found to be smaller than was observed with $ZnCl_2$. However, while there is more metallization of the Nvjp-1 in zinc acetate, residue coordination per Zn^{2+} did not show a significant increase, suggesting less sclerotization. This may explain the dynamic mechanical properties observed with zinc acetate treated Nvjp-1 hydrogels. This result suggests a potential role for the sequestration of acidic residues by protonated histidines at pH 5 in zinc chloride, where the salt bridges would create future metal coordination pockets within the protein by spatially localizing both coordinating carboxylates and imidazoles. These pockets would then become active metal coordination centers upon deprotonation of the imidazole side chains, a possibility supported by the observation that polar, acidic, and imidazole side chains are present together in many of the Zn^{2+} ligand fields. This may also explain the observed asymmetrical sclerotization response of Zn^{2+} treated hydrogels when comparing pH shifts from low to high or from high to low. In the latter case, the hydrogels may be unable to effectively rebind the relatively low Zn^{2+} levels released from the metal binding pockets as the pH level decreases. One central question related to the above mechanism is whether processing and metallization of Nvjp-1 occur at low pH in the natural system. A benefit related to the high histidine content of Nvjp-1 is its increased solubility at moderately low pH conditions. This property makes the protein easier to purify without column chromatography and process into hydrogels. The proximity of histidine's pK_a to neutrality would also make it easier for biological systems to affect the protonation state of this amino acid side chain in proteins through compartmentalized acidification. For example, HRPII, from the malarial parasite *Plasmodium falciparum*, has a histidine content that rivals that of Nvjp-1 and its biological function is to catalyze the formation of hemozoin crystals from degraded hemoglobin in the parasites acidified food vacuole.[34] Hydrolytic organelles like the *Plasmodium* vacuole can maintain pH environments of 5.5 which would increase the charge density of histidine rich proteins in a reversible manner. Secretory vesicles also acidify the intracellular compartment to pH 5.5 before fusion with the plasma membrane and release.[35] The steps involved in Nvjp-1 processing to form the sclerotized jaw are unknown, but it is not difficult to imagine that pH may play an important role in transport and metallization during the secretory process.

DFT calculations in vacuum predict binding of Zn^{2+} to polar and negatively charged residues. The binding to LYS in the Drude model is intriguing and requires further experimental and theoretical investigation. The energies from the Drude model are for Zn^{2+}−residue interactions in a complex environment. This suggests that an exhaustive combination of levels of theory and basis sets need to be explored in order to check if better agreement with theory and the Drude model can be obtained. Thus, development of ion parameters for use with protein residues is necessary for realistic simulations where good agreement between DFT and Drude ion−residue interaction energies may be obtained.

■ ASSOCIATED CONTENT

Supporting Information

The Supporting Information is available free of charge at https://pubs.acs.org/doi/10.1021/acs.jpcb.2c02807.

> Nvjp-1 *de novo* structure, protonation states of histidine and acidic residues, distance distributions of imidazole nitrogenes and carboxylic oxygens of acidic residues, root-mean-square deviation (RMSD) of the Nvjp-1 protein, Zn^{2+}−residue distance distributions, zinc coordination with polar and charged residues, examples of Zn coordination with carbonyl and hydroxyl oxygens, Zn^{2+}−residue interaction energies from DFT and the CHARMM-Drude model, equilibrium snapshots of Nvjp-1 with coordinating zinc ions, radius of gyration of Nvjp-1 as a function of time, normalized distribution of residues coordinating with Zn^{2+}, total number of coordinations of zinc ions (PDF)

■ AUTHOR INFORMATION

Corresponding Authors

Selemon Bekele − *Materials and Manufacturing Directorate, Air Force Research Laboratory, WPAFB, Ohio 45433-7131, United States; UES Inc., Dayton, Ohio 45432, United States*; Email: sbekele@ues.com

Rajiv Berry − *Materials and Manufacturing Directorate, Air Force Research Laboratory, WPAFB, Ohio 45433-7131, United States*; orcid.org/0000-0001-6355-8667; Email: rajiv.berry@us.af.mil

Authors

Kristi Singh − *Materials and Manufacturing Directorate, Air Force Research Laboratory, WPAFB, Ohio 45433-7131, United States; UES Inc., Dayton, Ohio 45432, United States*

Evan Helton − *Boonshoft School of Medicine, Wright State University, Dayton, Ohio 45435, United States*

https://doi.org/10.1021/acs.jpcb.2c02807
J. Phys. Chem. B 2022, 126, 6614−6623

Sanaz Farajollahi − *Materials and Manufacturing Directorate, Air Force Research Laboratory, WPAFB, Ohio 45433-7131, United States; UES Inc., Dayton, Ohio 45432, United States*

Rajesh R. Naik − *711th Human Performance Wing, Air Force Research Laboratory, WPAFB, Ohio 45433, United States;* Present Address: Mined XAI, Suite 200, 444 E. 2nd Street, Dayton Ohio, United States

Patrick Dennis − *Materials and Manufacturing Directorate, Air Force Research Laboratory, WPAFB, Ohio 45433-7131, United States*

Nancy Kelley-Loughnane − *Materials and Manufacturing Directorate, Air Force Research Laboratory, WPAFB, Ohio 45433-7131, United States;* orcid.org/0000-0003-2974-644X

Complete contact information is available at: https://pubs.acs.org/10.1021/acs.jpcb.2c02807

Notes

The authors declare no competing financial interest.

■ ACKNOWLEDGMENTS

We acknowledge funding from the Air Force Office of Scientific Research. P.D. is adjunct faculty in the Biochemistry and Molecular biology Department at Wright State University, Dayton, Ohio. The authors thank the DoD High Performance Computing Modernization Program for supercomputer resources.

■ REFERENCES

(1) Neal, J. A.; Oldenhuis, N. J.; Novitsky, A. L.; Samson, E. M.; Thrift, W. J.; Ragan, R.; Guan, Z. Large Continuous Mechanical Gradient Formation via Metal-Ligand Interactions. *Angew. Chem., Int. Ed.* **2017**, *56*, 15575−15579.

(2) Broomell, C. C.; Khan, R. K.; Moses, D. N.; Miserez, A.; Pontin, M. G.; Stucky, G. D.; Zok, F. W.; Waite, J. H. Mineral minimization in natureas alternative teeth. *J. R. Soc., Interface* **2007**, *4*, 19−31.

(3) Lichtenegger, H. C.; Birkedal, H.; Casa, D. M.; Cross, J. O.; Heald, S. M.; Waite, J. H.; Stucky, G. D. Distribution and Role of Trace Transition Metals in Glycera Worm Jaws Studied with Synchrotron Microbeam Techniques. *Chem. Mater.* **2005**, *17*, 2927−2931.

(4) Lichtenegger, H. C.; Schöberl, T.; Ruokolainen, J. T.; Cross, J. O.; Heald, S. M.; Birkedal, H.; Waite, J. H.; Stucky, G. D. Zinc and mechanical prowess in the jaws of Nereis, a marine worm. *Proc. Natl. Acad. Sci.* **2003**, *100*, 9144−9149.

(5) Birkedal, H.; Khan, R. K.; Slack, N.; Broomell, C.; Lichtenegger, H. C.; Zok, F.; Stucky, G. D.; Waite, J. H. Halogenated Veneers: Protein Cross-Linking and Halogenation in the Jaws of Nereis, a Marine Polychaete Worm. *ChemBioChem* **2006**, *7*, 1392−1399.

(6) Broomell, C. C.; Chase, S. F.; Laue, T.; Waite, J. H. Cutting Edge Structural Protein from the Jaws of *Nereis virens*. *Biomacromolecules* **2008**, *9*, 1669−1677.

(7) Chou, C. C.; Martin-Martinez, F. J.; Qin, Z.; Dennis, P. B.; Gupta, M. K.; Naik, R. R.; Buehler, M. J. Ion effect and metal-coordinated cross-linking for multiscale design of Nereis jaw inspired mechanomutable materials. *ACS Nano* **2017**, *11*, 1858−1868.

(8) Gupta, M. K.; Becknell, K. A.; Crosby, M. G.; Bedford, N. M.; Wright, J.; Dennis, P. B.; Naik, R. R. Programmable Mechanical Properties from a Worm Jaw-Derived Biopolymer through Hierarchical Ion Exposure. *ACS Appl. Mater. Interfaces* **2018**, *10*, 31928−31937.

(9) Partlow, B. P.; Hanna, C. W.; Rnjak-Kovacina, J.; Moreau, J. E.; Applegate, M. B.; Burke, K. A.; Marelli, B.; Mitropoulos, A. N.; Omenetto, F. G.; Kaplan, D. L. Highly tunable elastomeric silk biomaterials. *Adv. Funct. Mater.* **2014**, *24*, 4615−4624.

(10) Broomell, C. C.; Mattoni, M. A.; Zok, F. W.; Waite, J. H. Critical role of zinc in hardening of Nereis jaws. *J. Exp. Biol.* **2006**, *209*, 3219−25.

(11) Khan, R. K.; Stoimenov, P. K.; Mates, T. E.; Waite, J. H.; Stucky, G. D. Exploring Gradients of Halogens and Zinc in the Surface and Subsurface of Nereis Jaws. *Langmuir* **2006**, *22*, 8465−8471.

(12) Jing, Z.; Liu, C.; Cheng, S. Y.; Qi, R.; Walker, B. D.; Piquemal, J.; Ren, P. Polarizable Force Fields for Biomolecular Simulations: Recent Advances and Applications. *Annu. Rev. Biophys.* **2019**, *48*, 371−394.

(13) Williams, D. E. Alanyl dipeptide potential-derived net atomic charges and bond dipoles, and their variation with molecular conformation. *Biopolymers* **1990**, *29*, 1367−1386.

(14) Hensen, C.; Hermann, J. C.; Nam, K.; Ma, S.; Gao, J.; Holtje, H.-D. A combined QM/MM approach to protein-ligand interactions: polarization effects of theHIV-1 protease on selected high affinity inhibitors. *J. Med. Chem.* **2004**, *47*, 6673−6680.

(15) Alford, R. F.; et al. The Rosetta All-Atom Energy Function for Macromolecular Modeling and Design. *J. Chem. Theory Comput.* **2017**, *13*, 3031−3048.

(16) Huang, J.; Rauscher, S.; Nawrocki, G.; Ran, T.; Feig, M.; de Groot, B. L.; Grubmüller, H.; MacKerell, A. D., Jr CHARMM36m: an improved force field for folded and intrinsically disordered proteins. *Nat. Methods* **2017**, *14*, 71−73.

(17) Yu, H.; Whitfield, T. W.; Harder, E.; Lamoureux, G.; Vorobyov, I.; Anisimov, V. M.; MacKerell, A. D., Jr.; Roux, B. Simulating Monovalent and Divalent Ions in Aqueous Solution Using a Drude Polarizable Force Field. *J. Chem. Theory Comput.* **2010**, *6* (3), 774−786.

(18) Lopes, P. E. M.; Huang, J.; Shim, J.; Luo, Y.; Li, H.; Roux, B.; MacKerell, A. D., Jr. Polarizable Force Field for Peptides and Proteins Based on the Classical Drude Oscillator. *J. Chem. Theory Comput.* **2013**, *9* (12), 5430−5449.

(19) Li, H.; Ngo, V.; Da Silva, M. C.; Salahub, D. R.; Callahan, K.; Roux, B.; Noskov, S. Y. Representation of Ion-Protein Interactions Using the Drude Polarizable Force-Field. *J. Phys. Chem. B* **2015**, *119* (29), 9401−9416.

(20) Lin, F. Y.; Lopes, P. E. M.; Harder, E.; Roux, B.; MacKerell, A. D., Jr. Polarizable Force Field for Molecular Ions Based on the Classical Drude Oscillator. *J. Chem. Inf. Model.* **2018**, *58* (5), 993−1004.

(21) Lin, F. Y.; Huang, J.; Pandey, P.; Rupakheti, C.; Li, J.; Roux, B.; MacKerell, A. D., Jr. Further Optimization and Validation of the Classical Drude Polarizable Protein Force Field. *J. Chem. Theory Comput.* **2020**, *16* (5), 3221−3239.

(22) Jo, S.; Kim, T.; Iyer, V. G.; Im, W. CHARMM-GUI: A Web-based Graphical User Interface for CHARMM. *J. Comput. Chem.* **2008**, *29*, 1859−1865.

(23) Lee, J.; Cheng, X.; Swails, J. M.; Yeom, M. S.; Eastman, P. K.; Lemkul, J. A.; Wei, S.; Buckner, J.; Jeong, J. C.; Qi, Y.; Jo, S.; Pande, V. S.; Case, D. A.; Brooks, C. L.; MacKerell, A. D.; Klauda, J. B.; Im, W. CHARMM-GUI Input Generator for NAMD, GROMACS, AMBER, OpenMM, and CHARMM/OpenMM Simulations using the CHARMM36 Additive Force Field. *J. Chem. Theory Comput.* **2016**, *12*, 405−413.

(24) Phillips.; et al. Scalable molecular dynamics on CPU and GPU architectures with NAMD. *J. Chem. Phys.* **2020**, *153*, 044130.

(25) Lamoureux, G.; Harder, E.; Vorobyov, I.; MacKerell, A. D., Jr.; Roux, B. A polarizable model of water for molecular dynamics simulations of biomolecules. *Chem. Phys. Lett.* **2006**, *418*, 245−249.

(26) Darden, T.; York, D.; Pedersen, L. Particle mesh Ewald: An NlogN method for Ewald sums in large systems. *J. Chem. Phys.* **1993**, *98*, 10089.

(27) Essmann, U.; Perera, L.; Berkowitz, M. L.; Darden, T.; Lee, H.; Pedersen, L. G. A smooth particle mesh ewald method. *J. Chem. Phys.* **1995**, *103*, 8577.

(28) Allen, M. P.; Tildesley, D. J. *Computer Simulation of Liquids*; Oxford University Press: Oxford, U.K., 2004.

(29) Nose, S. A unified formulation of the constant temperature molecular dynamics methods. *J. Chem. Phys.* **1984**, *81*, 511.
(30) Hoover, W. G. Canonical dynamics: Equilibrium phase-space distributions. *Phys. Rev.* **1985**, *A31*, 1695−1697.
(31) Søndergaard, C. R.; Olsson, M. H. M.; Rostkowski, M.; Jensen, J. H. Improved Treatment of Ligands and Coupling Effects in Empirical Calculation and Rationalization of pKa Values. *J. Chem. Theory Comput.* **2011**, *7* (7), 2284−2295.
(32) Olsson, M. H. M.; Søndergaard, C. R.; Rostkowski, M.; Jensen, J. H. PROPKA3: consistent treatment of internal and surface residues in empirical pKa predictions. *J. Chem. Theory Comput.* **2011**, *7* (2), 525−537.
(33) Frisch, M. J.; Trucks, G. W.; Schlegel, H. B.; et al. *Gaussian 16*, revision C.01; Gaussian, Inc.: Wallingford, CT, 2019.
(34) Sullivan, D. J.; Gluzman, I. Y.; Goldberg, D. E. Plasmodium hemozoin formation mediated by histidine-rich protein. *Science* **1996**, *271*, 219−222.
(35) Casey, J. R.; Grinstein, S.; Orlowski, J. Sensors and regulators of intracellular pH. *Nat. Rev. Mol. Cell Biol.* **2010**, *11*, 50−61.

https://doi.org/10.1021/acs.jpcb.2c02807
J. Phys. Chem. B 2022, 126, 6614−6623